Int. J. Multiphase Flow Vol. 16, No. 6, pp. 935–949, 1990
Printed in Great Britain.

0301-9322/90 $3.00 + 0.00

PARTICLE–TURBULENCE INTERACTION IN A BOUNDARY LAYER

M. RASHIDI, G. HETSRONI† and S. BANERJEE
Department of Chemical and Nuclear Engineering, University of California at Santa Barbara, Santa Barbara, CA 93106, U.S.A.

(*Received* 27 *March* 1990; *in revised form* 24 *July* 1990)

Abstract—Particle–turbulence interaction in wall turbulent flows has been studied. A series of experiments varying particle size, particle density, particle loading and flow Re has been conducted. The results show that the larger polystyrene particles (1100 μm) cause an increase in the number of wall ejections, giving rise to an increase in the measured values of the turbulence intensities and Reynolds stresses. On the other hand, the smaller polystyrene particles (120 μm) bring about a decrease in the number of wall ejections, causing a decrease in the measured intensities and Reynolds stresses. These effects are enhanced as the particle loading is increased. It was also found that the heavier glass particles (88 μm) do not bring about any significant modulation of turbulence. In addition, measurements of the burst frequency and the mean streak-spacing show no significant change with increase in particle loading. Based on these observations, a mechanism of particle transport in wall turbulent flows has been proposed, in which the particles are transported (depending on their size, density and flow Re) by the bursting events of the wall regions.

Key Words: particles, turbulence, boundary layer

INTRODUCTION

Turbulent fluid flows laden with solid particles are poorly understood, though they are very common in nature and technology, i.e. transport of pollutant in rivers, sediment transport in oceans and a variety of process equipment such as cyclones, precipitators, aerosol reactors etc. The addition of particulate matter to turbulent flows increases the complexity of the phenomena and hinders modeling or theoretical treatment.

Particle-laden turbulent flows have been investigated in several experiments with the main interest usually being in particle dispersion by turbulence (e.g. Soo *et al.* 1960; Snyder & Lumley 1971; Wells & Stock 1983).

Several experiments of particle-laden fully-developed pipe flow and free shear flow have shown that particles cause modulation of the turbulence in these flows. Particles with $Re_p < 100$ would suppress the turbulence and have a similar effect as to an increase in viscosity. Hetsroni (1989) suggested that particles with $Re_p > 400$ would enhance the turbulence of the mainstream because of vortex shedding. All the experimental data available collaborate this model and are summarized therein.

The interaction between particulate matter and the turbulence of the carrier fluid in boundary layers has been investigated since Bagnold (1941) shed some light on the phenomena. However, not until the structure of the turbulence near a solid wall is better understood can progress be made in understanding the motion of particles in turbulent flows.

It is now known that a boundary (whether it is a wall or free surface) suppresses the normal components of turbulent fluctuations due to the kinematic constraints, and generates organized structure if a mean shear is imposed on it. When the shear rate is increased, alternating high-speed and low-speed regions are observed near the boundary. These observations were first made by Kline *et al.* (1967) near a solid wall and later by Rashidi & Banerjee (1990a) near a sheared gas–liquid interface. It is conjectured that the low-speed/high-speed flow pattern results from the counter-rotating streamwise vortex pairs that are broken up periodically near the wall (or near the sheared interface), thus initiating the bursting process. The bursting process is a randomly occurring event consisting of a gradual local liftup of the low-speed streaks, sudden oscillation and ejection of

†Permanent address: Department of Mechanical Engineering, Technion—Israel Institute of Technology, Haifa, Israel.

low-momentum fluid from the wall region into the main stream. This is then followed by an insweep of high-momentum fluid into the wall region. This spectacular phenomenon of bursting has been shown to be responsible for most of the turbulence energy production and to be the major contributor to the transport of Reynolds stresses.

It is clear that particulate matter suspended in the boundary layer interacts with these dominant structures, and that this interaction may be quite complex. Grass (1974) recorded the details of the suspension process in a turbulent boundary layer on a flat plate. He observed that sand particles were carried up from the bed region through virtually the total boundary layer thickness. Later, Sumer & Deigaard (1981) made some measurements on the motion of 3.0 mm dia particles near a wall, using a photogrammetric system. They traced the motion of a single particle suspended in water in a horizontal channel. They found that, with a smooth bottom wall, the measured kinematical quantities characterizing the particle motion were in accord with available information on the bursting phenomena, as described above, suggesting that this is perhaps a mechanism to cause particle suspension in the flow.

Dyer & Soulsby (1988) have similarly shown the importance of the bursting phenomenon on the transport of the particles on the ocean floor. The periodic ejection and insweep events associated with the bursting process have been captured in the instantaneous measurements of the Reynolds stress. This is seen as a sudden rise in the Reynolds stress magnitude of up to 30 times the mean Reynolds stress. In the ocean, these events are visible as swirls of sand that are lifted up above the ocean floor. Furthermore, it has been observed by Taylor & Dyer (1977), Itakura & Kishi (1980) and Soulsby & Wainwright (1987) that the particle movement affects the fluid velocity profile. Depending on the particle size and the particle velocity, the fluid velocity profiles may become concave or convex.

Rogers & Eaton (1989) measured the response of solid particles to a vertical turbulent boundary layer in air, using a low concentration of 50 and 90 μm glass particles. They found that the r.m.s. velocity fluctuations of both particle sizes nearly equaled the streamwise turbulence intensity of the flow, but the turbulence intensity of the particles in the normal direction was strongly attenuated, i.e. they were much lower than the fluid's. The power spectra showed that for the normal fluctuations the power spectrum shifts to higher frequencies relative to the streamwise fluctuations, therefore indicating that the particles did not closely follow the fluid fluctuations in the normal direction. Rogers & Eaton also used 70 μm copper particles to create a greater particle mass loading of 20%. The presence of these particles tended to suppress turbulence, with the degree of turbulence suppression being a function of the distance downstream in the boundary layer. They attributed the turbulence suppression to an increase in the dissipation. However, they were unable to clarify their results in light of the observed dominant flow events near the wall.

Yung *et al.* (1989) investigated the interaction of the turbulent bursts and the deposited particles within the viscous sublayer near the wall. They carefully placed spherical particles of polystyrene and glass (50 μm dia) on the wall so that the particles were completely submerged within the viscous sublayer. Their flow visualization experiments showed that the bursting phenomenon has an insignificant effect on re-entrainment of the deposited particles within the viscous layer. It was shown that only about 1% of the particles are lifted up into the flow by the wall bursts. However, as the size of the particles increased, the number of the re-entrained particles also increased. Based on these results they concluded that, in contrast to the previous hypothesis, the turbulent bursts are not effective to re-entrain the particles within the experimental range of $0.5 < d^+ < 1.3$, where d^+ is the non-dimensional particle diameter (du_*/ν). On the other hand, as d^+ increases, the importance of turbulent bursts in particle re-entrainment is substantially increased.

Cleaver & Yates (1973, 1975, 1976), in an attempt to model the particle transport in turbulent flows, suggested that the particles are re-entrained by the wall ejection events while they are deposited by the insweep events. Their model had some agreement with the limited experimental data in predicting the particle deposition and re-entrainment rates. Although their model and some recent theoretical attempts have been based on some characteristics of the bursting phenomenon, there is still not enough experimental evidence as to the details of the turbulence–particle interactions for any realistic modeling of this problem.

In the present paper, particle–turbulence interaction in wall flows has been studied in a horizontal open channel. Experiments have been conducted varying particle size, particle density, particle

loading and flow Re. The objective is to better understand the influence of the particles on the dominant flow structures and the effect of these structures on the particle motion near the wall. In particular, the following issues are investigated:

- Do the particles affect the turbulence characteristics such as ejections and bursts frequencies, streak-spacing and magnitude of the ejections and, if so, how does this influence turbulence quantities like mean velocity profiles, turbulence intensities and Reynolds stresses?
- In light of the above findings, can a mechanism of particle transport be proposed in which the particle entrainment and deposition are better understood and related to the underlying bursting events near the wall?

EXPERIMENTAL FACILITIES AND PROCEDURES

The experiments were conducted in a Plexiglas rectangular channel with liquid recirculating facilities. The channel is made up of four equal sections and is 4.0 m long, 0.20 m wide and 0.15 m deep. It was designed so that, at the test section, flow was fully developed with an aspect ratio large enough to be free from wall effects at the centre (figure 1).

The liquid is circulated by a centrifugal pump and the flow rate is measured using a Venturi meter. The liquid is filtered continuously to remove solids $>5\,\mu$m. Measurements of liquid temperature were performed at the entrance, the exit and the test section of the channel with thermocouples placed on the side walls and with a set of precision mercury thermometers placed in the channel. Great care was taken to eliminate wave formation at the inlet and reflections from the outlet. As a result, the flow was introduced into the inlet tank through several inlet holes in order to provide a setup that produced high flow rates with no significant interfacial waves. Efforts were also made to maintain a constant average flow and temperature throughout each run.

The particles (glass or polystyrene) were introduced in the flow at about 0.60 m upstream from the test section. This was done using a 3 mm dia tubing placed in the center of the channel and at the center of the flow depth. A known solution of each particle size was made in a separate

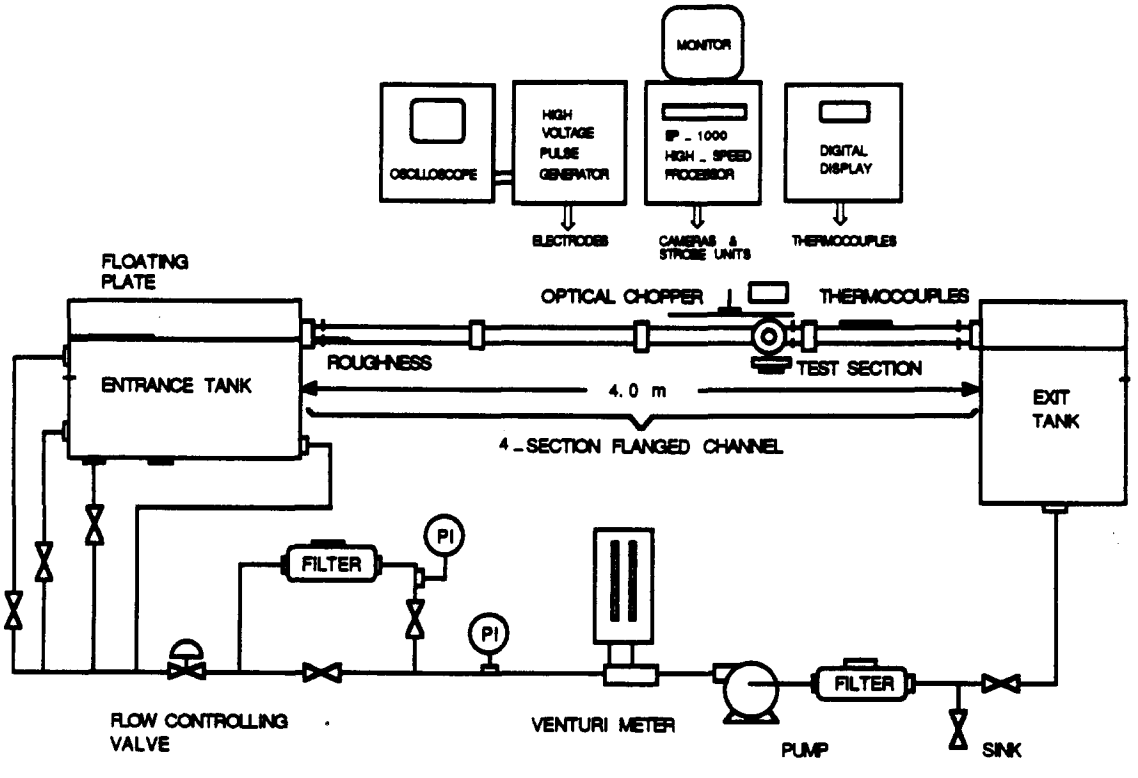

Figure 1. Experimental facility and arrangement of measurement devices.

mixing vessel, and was added into the flow by a variable-speed peristaltic pump, such that the particles were introduced in the flow with a known concentration and flow rate. The particle loading was controlled by changing the solution concentration or the pump's speed. The added particles were collected at the exit of the channel using a 50 μm mesh filter. The effect of the tube presence, tube height location and particle acceleration on the mean flow velocity was later checked experimentally and theoretically to ensure a minimal disturbance of the flow. This was done theoretically by evaluating the appropriate length between the test section and the tube that provided negligible tube wake effect and enough time for particles to accelerate to the mean flow velocity. In addition, experiments were conducted with and without the tube presence to ensure that the tube wake effect had no influence on the visualized instantaneous velocity profiles. The effect of tube height location was also checked experimentally by changing the height of the tube with respect to the bottom wall and observing the effect on the measured wall ejection frequencies at the test section. This was done for three locations, $y/h = 0.1$, 0.5 and 0.9, and the effect was found to be insignificant for the present experimental conditions.

Measurements were made in liquid streams primarily by flow visualization. This was done through the use of very small (~ 20 μm dia) oxygen bubble tracers (Rashidi & Banerjee 1988) that were photographed using a high-speed video analyzer and alternatively a 35 mm camera with mechanically chopped flashes. The chopper had a constant speed of about 3700 rpm. It was designed so that several high-intensity beams of collimated light were produced by chopping a single flash. This resulted in well-spaced traces of both bubbles and particles in a film frame from which flow and particle velocities were found by image processing. The bubbles were produced from two platinum wires (25 μm dia) using a high-voltage pulse generator (20–200 pulse/s with a pulse duration of 1–5 ms at up to 300 V). One wire was placed horizontally parallel to the bottom of the channel and aligned in the spanwise direction (and could be moved up and down between the wall and interface), while the other wire was held vertically across the channel.

The high-speed video recording system was a two-camera Kodak (Spin Physics) EP-1000 motion analyzer. It was used with both conventional and fiber-optic synchronized-strobe units. The system has a maximum full-screen capability of 1000 frame/s and a maximum split-screen capability of 6000 frame/s. In these experiments, data were generally recorded at 250 frame/s. The recorded data could be played back in slow motion as well as in single frames for detailed data analysis. The split-screen capability allowed one camera to be used to record the flow structures in the horizontal plane, while the other captured the structures in the vertical plane.

EXPERIMENTAL CONDITIONS

The experimental runs were conducted in the described flow facilities. The flow conditions are summarized in table 1. The experiments were done at four different Reynolds (and Froude) numbers under hydraulically subcritical conditions. Reynolds numbers based on flow depth and based on equivalent diameter are listed in table 1. For the runs discussed here, it was possible to form a turbulent liquid flow with no significant interfacial waves. Therefore, particle–turbulence interaction was studied without the influence of interfacial waves. The values of the wall friction velocity, presented in table 1, were evaluated from the measured velocity profiles and the Blasius formula. Both methods gave similar results.

Particle characteristics are listed in table 2. Both spherical polystrene and glass particles were used in this study. The polystyrene particles had sp. gr. 1.03 ± 0.02 and were employed in four different sizes of about 120, 220, 650 and 1100 μm dia. The glass particles had sp. gr. 2.50 ± 0.05 and were about 88 μm dia. Experiments were conducted at four different particle loadings, defined as Q_P/Q_F (where Q_P and Q_F are the particle and fluid volumetric flow rate, respectively); these were 0, 0.9×10^{-4}, 1.8×10^{-4} and 3.6×10^{-4}. The values of Q_P/Q_F were evaluated first from the measured values of particle and fluid flow rates, but later verified from the recorded video sequences of the flow field. The latter was done from the measurement of particle concentrations (from video sequences) averaged throughout each experimental run.

Table 1. Flow conditions

Reynolds number, Re ($\mathbf{u}_M h/\nu$)	Flow depth, h (cm)	Equivalent diameter, D (cm)	Kinematic viscosity, $\nu \times 100$ (cm^2/s)	Mean velocity, $\mathbf{u}_M$ (cm/s)	Friction velocity, u_* (cm/s)	Froude number, Fr ($\mathbf{u}_M/\sqrt{gh}$)	Reynolds number, Re_D ($\mathbf{u}_M D/\nu$)
7500	2.75 ± 0.05	8.63	0.848	$23.6 \pm 2.3\%$	1.29	0.45	24,000
5000	2.75	8.63	0.839	15.6	0.90	0.30	16,000
3500	2.75	8.63	0.830	11.0	0.66	0.21	11,500
2500	2.75	8.63	0.821	7.7	0.46	0.15	8000

Table 2. Particle characteristics

Particle type	Diameter (μm)	Specific gravity	Particle geometry	Loading, $Q_P/Q_F \times 10^4$
Polystyrene	120	1.03 ± 0.02	Spherical	0.9, 1.8, 3.6
Polystyrene	220	1.03	Spherical	1.8
Polystyrene	650	1.03	Spherical	1.8
Polystyrene	1100	1.03	Spherical	0.9, 1.8, 3.6
Glass	88	2.50 ± 0.05	Spherical	1.8

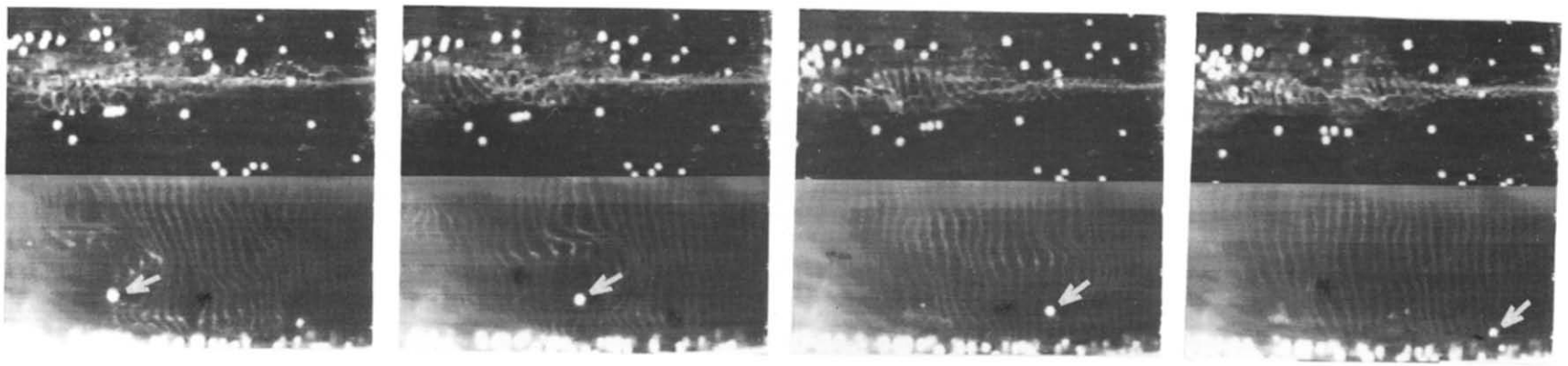

Figure 2. Sequential pictures (right to left) of wall burst interaction with the polystyrene particles of 1100 μm (indicated by the arrows) at Re = 5000. The time interval between the photographs is 0.12 s.

RESULTS

A. Turbulence–particle interaction

To investigate the dominant structures near the wall and their interactions with the particles, the high-speed video system was used. The system was used to view simultaneously the near-wall regions in the horizontal plane (upper portion of the screen) and the particle–burst interactions in the vertical plane (lower portion of the screen). Figure 2 illustrates a sequence of pictures obtained this way for Re = 5000 and 1100 μm polystyrene particles. As seen from these pictures and many other video sequences, the ejections originating at the wall clearly interact with the particles, and generally lift them up into the bulk flow. The ejected particles, after moving up a distance from the wall, lose their vertical momentum and return toward the wall. The cycle then repeats itself.

In order to study the details of turbulence–particle interaction, the influence of particles on the wall ejections was examined. For each run, a video sequence of at least 22,000 frames ($\sim$3 min) was recorded. From this sequence, about 100 wall ejections were measured. The measurements of wall ejection frequency were done from the EP-1000 recorded video sequences that provided the time and frame number of the events. In the video sequences, the wall ejections are characterized by the liftup and ejection of vortical structures in the upper portion of the screen (horizontal plane). This is seen in the lower screen (vertical plane) as a deceleration of instantaneous velocity profiles near the wall followed by a sudden ejection from the wall region. The ejections were measured at a fixed location 30 mm downstream from the vertical wire at $y^+ \approx 20$ to 30 (where $y^+ = yu_*/\nu$ is the distance from the wall non-dimensionalized by the wall shear velocity, u_*, and kinematic viscosity, ν).

Figure 3 shows the effect of particle size on the average time between wall ejections or ejection periods (T_E) as a function of fluid Re. Here, the values of T_E are measured as described above and are normalized by the ejection periods obtained for the flow with no particles, $T_E^* = (T_E/T_{E\,\text{no loading}})$. As seen from figure 3, the larger polystyrene particles of 1100 μm dia cause an increase in the number of ejections near the wall. The effect is slightly enhanced as Re decreases. This is, perhaps, because at lower Re particles tend to settle down at the bottom of the channel and interact with the organized structures more frequently. Figure 4 illustrates this point, i.e. the percentage particle concentration near the wall increases as the particle size increases. On the other hand, the smaller polystyrene particles of 120 μm cause a slight decrease in the number of wall ejections. This effect is more evident for the highest Re. This could be due to the fact that the smaller particles tend to follow the flow more closely, though there is still a relative velocity between the particles and the fluid. This relative velocity and the existence of velocity gradients around the particles increase the energy dissipation. This is similar to the effect that one observes if viscosity is increased. Looking at the results for the runs with glass particles, it appears that the presence of the glass particles does not enhance or reduce the observed ejection frequencies. The video sequences show that the 88 μm glass particles, due to their smaller size and higher density, roll beneath the dominant wall structures, therefore not causing any changes in the number of wall ejections.

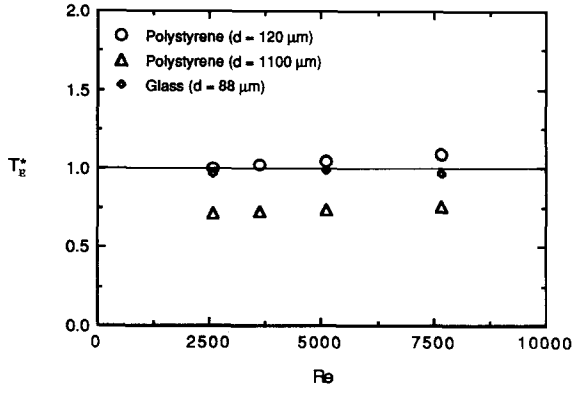

Figure 3. Effect of particles on the average, non-dimensional time between wall ejections, $T_E^* = (T_E/T_{E\,\text{no loading}})$, as a function of fluid Re. $Q_P/Q_F = 1.8 \times 10^{-4}$, where Q_P and Q_F are the particle and fluid volumetric flow rates, respectively.

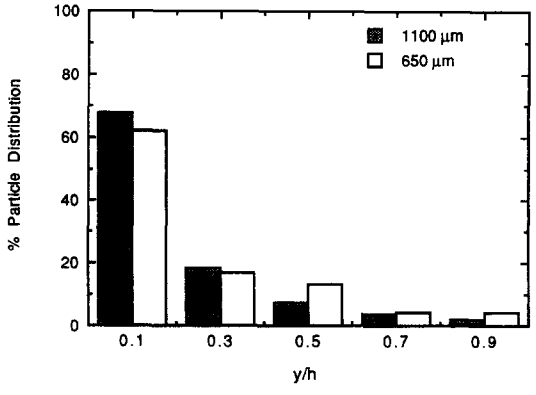

Figure 4. Particle distribution as a function of the non-dimensional distance from the wall.

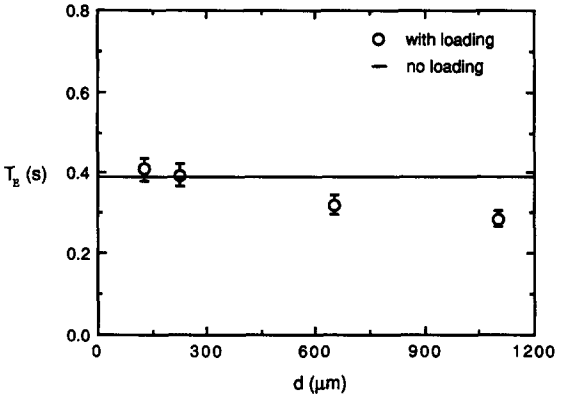

Figure 5. Effect of particle size on the average time between wall ejections, T_E, at Re = 5000, $Q_P/Q_F = 1.8 \times 10^{-4}$. The uncertainty in the values of T_E is $\pm 7\%$ at the 95% confidence level for 100 ejection measurements.

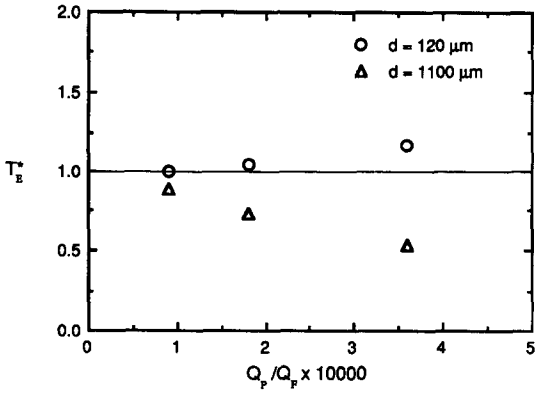

Figure 6. Effect of particle loading on the average non-dimensional time between wall ejections, T_E^*, at Re = 5000.

Similarly, it is shown in figure 5 that for Re = 5000 and constant particle loading (polystyrene particles), the number of wall ejections also increases with particle size. This is seen for particle sizes of $d > 300\ \mu$m. For smaller particles of $d < 300\ \mu$m, there is a slight decrease in the number of wall ejections.

In order to examine the observed trend further, the effect of particle loading on the number of wall ejections was also studied. Figure 6 shows the variations of ejection period (T_E) with the particle loading ratio (Q_P/Q_F) for Re = 5000 and polystyrene particle sizes of 120 and 1100 μm. As seen from this figure, the previous trend is intensified as the particle loading is increased. Namely, for the larger particles of 1100 μm dia the number of wall ejections is increased substantially as the particle loading is increased. However, for the smaller particles of 120 μm dia, the increase in the particle loading causes a greater decrease in the number of ejections near the wall.

The effect of particle loading on the structures near the wall was also studied with respect to the low-speed/high-speed streaks of the wall regions. Figure 7 illustrates the distribution of 1100 μm particles and their interactions with the low-speed/high-speed streaks that form near the wall. As seen from this sequence and others, particles generally accumulate in the low-speed regions of the streaks and then are taken away by the wall ejections into the bulk flow. Furthermore, it appears that the wall streaks have the same characteristics as those observed for the runs with no particles. Figures 8(a,b) show the variation of the mean non-dimensional spanwise streak-spacing, $\lambda^+ = \lambda u_*/\nu$, as a function of particle loading for both 120 and 1100 μm particles at $y^+ = 5$. As before, for each run a video sequence of at least 22,000 frames ($\sim$3 min) was recorded and from this sequence 60–80 frames were analyzed. The reported mean streak-spacings correspond to at least 200 counts of the streaks. As seen from this figure, the change in particle loading does not influence the average spacing of the wall streaks. It appears that, for both 120 and 1100 μm particles, the mean spacing of the streaks non-dimensionalized with the wall shear velocity (u_*) and kinematic viscosity (ν) changes very little with increases in particle loading and exhibits consistent values of $\lambda^+ \approx 100$ at $y^+ = 5$. This is indeed a significant finding, since the particle introduction influences the frequency of wall ejections but has a negligible effect on the streaks' appearance and their spacing.

In order to investigate the particle–turbulence interaction further, the effect of particle loading on the burst frequency was also examined. A burst consists of several closely grouped ejections that are associated with the formation and complete breakdown of a vortex-like structure near the wall (see subsection C). From the video sequence of each run, about 100 wall bursts were measured and, as before, the burst frequencies were evaluated. Figure 9 shows the effect of particle size on the average time between wall bursts or burst periods (T_B) for Re = 5000. Here, the values of T_B are compared with the burst periods obtained for flow with no particles. It appears from this figure that the burst frequency is affected very little by the addition of the particles to the flow. This is interesting, since it implies that the particles do not affect the overall cycle of the bursting process, however, they cause an alteration in the number of ejections within a burst.

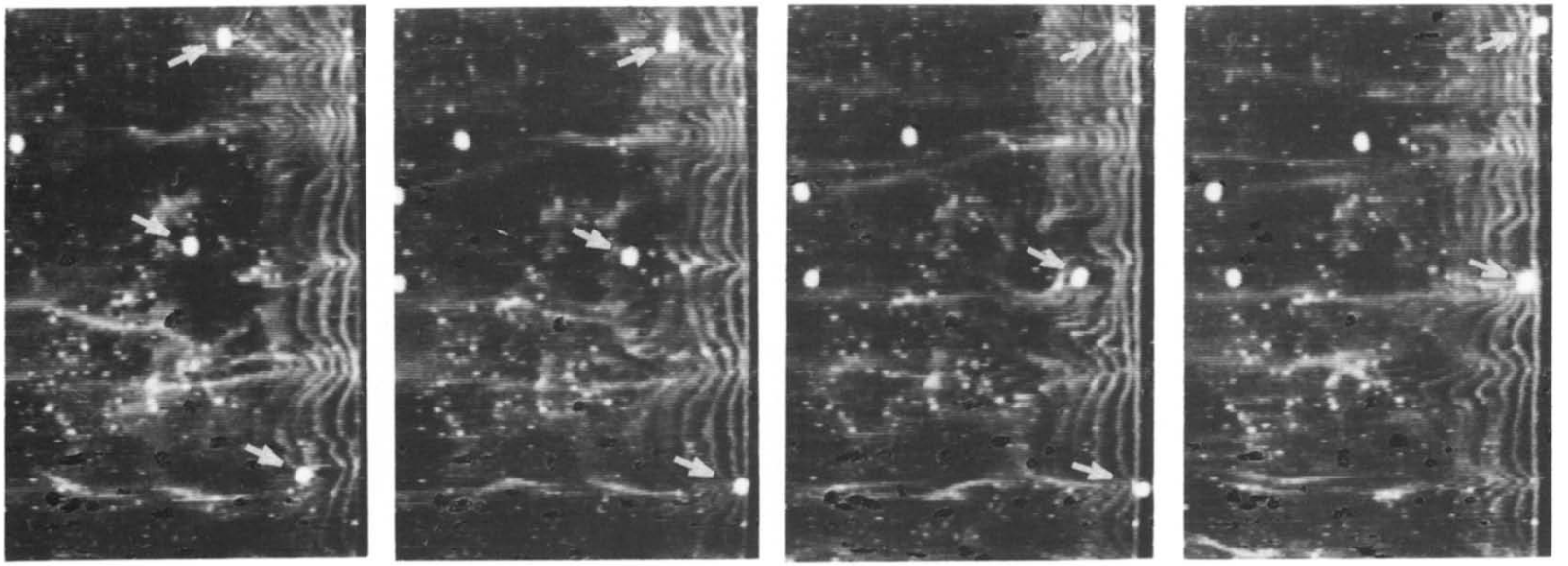

Figure 7. Illustration (right to left) of particle distributions with respect to the low-speed/high-speed streaks of the wall regions; $d = 1100\ \mu$m particles, Re = 5000, $y^+ = 5 \pm 1$. The time interval between the photographs is 0.08 s.

Table 3. Ejection velocity

Run	Particle type	Particle diameter (μm)	d^+ ($u_* d/\nu$)	Particle loading, $Q_P/Q_F \times 10^4$	Mean dimensionless ejection	Re ($\mathbf{u}_M D/\nu$)
1	Polystyrene	120	1.3	0.9	1.03	5000
2	Polystyrene	120	1.3	3.6	1.12	5000
3	Polystyrene	1100	11.8	0.9	0.99	5000
4	Polystyrene	1100	11.8	3.6	0.82	5000
5	Glass	88	0.9	1.8	1.00	5000

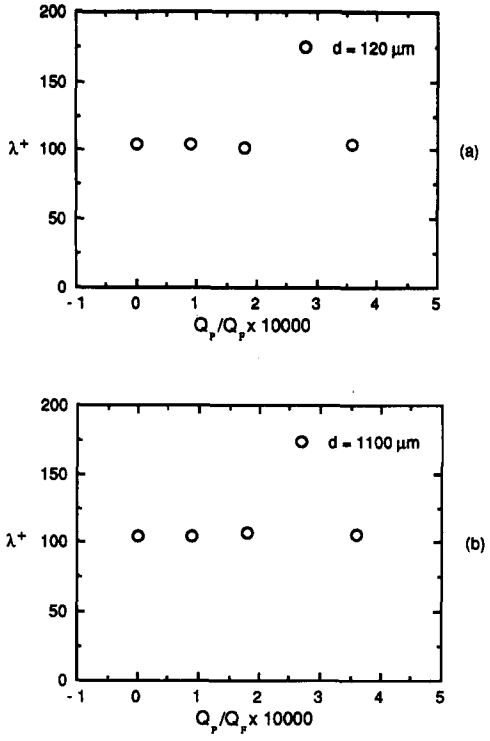

Figure 8. Variation of mean non-dimensional spanwise streak-spacing, $\lambda^+ = \lambda u_*/\nu$ as a function of particle loading; Q_P/Q_F at Re = 5000 and $y^+ = 5 \pm 1$. (a) 120 μm particles; (b) 1100 μm particles. The uncertainty in the values of λ^+ is about $\pm 7\%$ at the 95% confidence level for 200 measurements.

The question that arises at this point is that if the ejection frequencies are changed by the particle loading, how does this effect the ejection velocities? In order to answer this question, the values of ejection velocities were measured and averaged for some runs (table 3). The listed values of ejection velocities were evaluated from the video sequences of each run at $y^+ = 20$ to 30 and were averaged for 100 measurements. These values are normalized by the mean ejection velocity of the run with the glass particles. It appears from these results that as particle loading is increased, the mean ejection velocity is also increased for the 120 μm polystyrene particles. However, the increase in particle loading decreases the mean ejection velocity for the 1100 μm polystyrene particles. This demonstrates that although the particle loading increases (1100 μm particles) or decreases (120 μm particles) or decreases (120 μm particles) the ejection frequencies, it also causes a reduction (1100 μm particles) or an enhancement (120 μm particles) of ejection velocities, respectively.

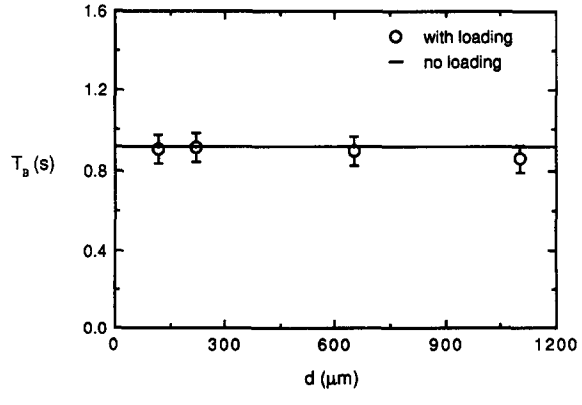

Figure 9. Effect of particle size on the average time between wall bursts, T_B, at Re = 5000, $Q_P/Q_F = 1.8 \times 10^{-4}$. The uncertainty in the values of T_B is $\pm 8\%$ at the 95% confidence level for 100 burst measurements.

The above results show that particle introduction in the flow does not affect the overall qualitative cycle of bursting, but rather changes the frequency and velocity of the ejections within a burst. In other words, the presence of particles affects the transport mechanism of turbulence energy from the wall region to the bulk flow. It is known that turbulence production energy peaks near the wall and, furthermore, virtually all of this energy occurs during the bursting process (Kim *et al.*, 1971). The particle loading changes the process by which this energy is transported from the wall region to the bulk flow.

B. Turbulence–particle statistics

Measurements of fluid and particle velocity profiles were obtained by image processing of the slides taken using the flash photography technique described above. The sample sizes were limited to about 250 and 100 instantaneous fluid and particle velocity profiles, respectively. Mean velocity profiles evaluated in this way are plotted for some runs in figure 10. It appears from this figure that all runs exhibit a similar profile through the flow depth. However, near the interface there is a slight enhancement of the mean velocity for the runs with the larger polystyrene particles of size 1100 μm and a very slight reduction in the mean velocity for the runs with the smaller polystyrene particles of 120 μm. Figure 11 shows the data plotted in terms of $u^+ = (\mathbf{u}/u_*)$ and $y^+ = (yu_*/\nu)$. As seen from this figure, the data exhibit log-law profiles through most of the flow depth and can be described by

$$u^+ = 2.44 \ln y^+ + 5.0.$$

However, near the interface, for the cases with high particle loading there is a noticeable deviation from the log-law profile. This deviation is related to the earlier findings of changes in the wall ejection frequencies as a result of particle introduction. The larger particles of 1100 μm cause a substantial increase in the number of wall ejections, whereas the smaller particles of 120 μm bring about a decrease in the number of these ejections. Since the structures near the wall have a direct influence on the mean velocity profile, the observed deviations of the mean velocity profiles are perhaps a result of the changes in the wall ejection frequencies.

In addition to the fluid velocity profiles, particle velocity profiles were also evaluated for all polystyrene particles. Figure 12 shows the mean particle velocity profiles of various size particles as a function of non-dimensional distance from the wall. As seen from this figure, the smaller particles of 120 μm have almost the same velocities as the fluid velocities. However, as the size increases, the particles move at slower mean velocities than the fluid velocities. The deviation is observed to be greater near the wall where a larger velocity gradient exists. This agrees with the findings of Sumer & Deigaard (1981). Similarly, the relative particle–fluid velocities were also evaluated from each slide. Figure 13 illustrates the relative velocity profiles as a function of

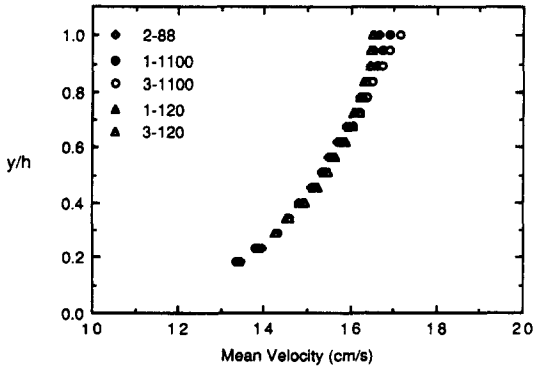

Figure 10. Mean streamwise velocity profiles as a function of the non-dimensional distance from the wall. ◇, glass particle of 88 μm, $Q_P/Q_F = 1.8 \times 10^{-4}$; ●, polystyrene particles of 1100 μm, $Q_P/Q_F = 0.9 \times 10^{-4}$; ○, polystyrene particles of 1100 μm, $Q_P/Q_F = 3.6 \times 10^{-4}$; ▲, polystyrene particles of 120 μm, $Q_P/Q_F = 0.9 \times 10^{-4}$; △, polystyrene particles of 120 μm, $Q_P/Q_F = 3.6 \times 10^{-4}$.

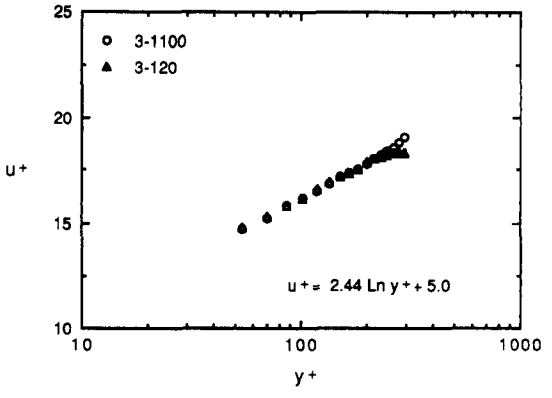

Figure 11. Dimensionless mean velocity profiles, $u^+ = (\mathbf{u}/u_*)$ vs $y^+ = (yu_*/\nu)$ for 120 and 1100 μm polystyrene particles. (Symbols have the same meaning as in figure 10.)

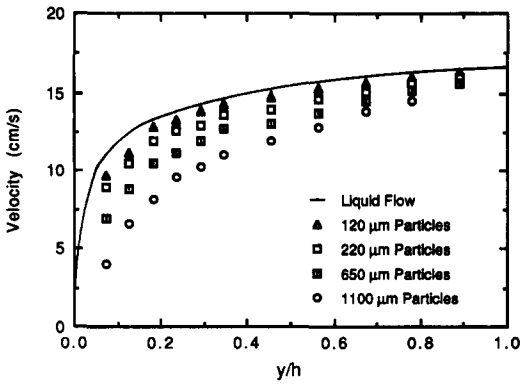

Figure 12. Mean particle velocity profiles as a function of the non-dimensional distance from the wall.

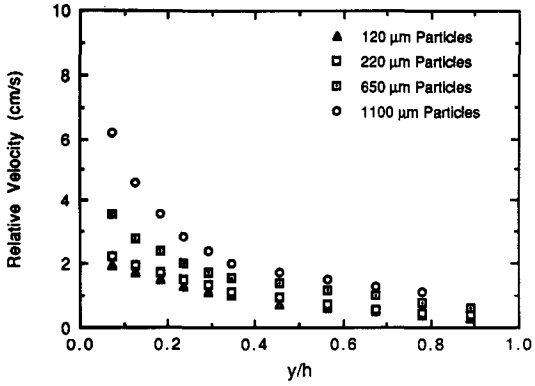

Figure 13. Mean relative (particle–fluid) velocity profiles as a function of the non-dimensional distance from the wall. The relative velocity profiles were averaged from the absolute values of the differences between instantaneous fluid and particle velocities.

non-dimensional distance from the wall. These values were averaged from the absolute values of differences between instantaneous fluid and particle velocities. It can be seen that the relative velocity profiles are in agreement with the results shown in the previous figure. Namely, as the particle diameter increases the relative velocity also increases, and it is largest near the wall. This trend is understandable, since as the particle size increases the particle response to the fluid velocity decreases giving rise to an increase in the relative velocities, i.e. the particles of 1100 μm have a relaxation time (the time it takes for a particle at rest to be accelerated to within $\sim$63% of the fluid velocity) of about 0.1 s, while the relaxation time for the 120 μm particles is only about 0.001 s.

In order to further investigate the particle–turbulence interactions, the values of turbulence intensities were also evaluated. Figure 14 shows plots of the streamwise intensities ($u' = \sqrt{\overline{u^2}}$), the vertical intensities ($v' = \sqrt{\overline{v^2}}$) and the Reynolds stresses ($\overline{uv}$) non-dimensionalized with the friction velocity, u_* for six runs. Here, u and v are the fluctuating velocity components in the streamwise (x) and vertical (y) directions. It appears from these plots that the intensity profiles all have the same general trends as the run with no particles. That is, the vertical component is damped near the interface, causing an enhancement of the streamwise component in the same regions. However, the magnitudes of the intensities are modified as a result of particle addition. As seen from these plots, glass particles of 88 μm dia have an almost insignificant effect on the turbulence intensities of the flow and give similar profiles to the run with no particles. On the other hand, the introduction of polystyrene particles causes a considerable change in the values of the intensities. It appears that the larger particles of size 1100 μm cause an enhancement of the streamwise intensities, while the smaller particles of size 120 μm cause a suppression of these intensities. Furthermore, it is observed that the effect is intensified as the particle loading is increased. Looking at the corresponding vertical turbulence intensities, a similar effect is observed. Namely, the larger polystyrene particles cause an increase in the vertical component of intensities, whereas the smaller polystyrene particles cause a decrease in these intensities.

The observed trends in the intensity profiles can be best understood from the corresponding Reynolds stress profiles. These profiles indicate that for the larger polystyrene particles of 1100 μm, the Reynolds stress values increase substantially near the wall and throughout the flow depth. On the other hand, the smaller polystyrene particles of 120 μm cause a decrease in the Reynolds stress values. Furthermore, the effect is enhanced as the particle loading is increased. These results are in agreement with the wall ejection measurements shown in the previous section—the larger polystyrene particles, due to their interactions with the wall structures, cause an increase in the wall ejection frequencies which, as a result, give rise to the enhancement of the intensities and Reynolds stresses. However, the smaller polystyrene particles cause the opposite effect on both the wall ejection frequencies and the resulting intensity and Reynolds stress measurements. As noted, the heavier glass particles do not bring about any considerable change in these results. The video pictures show that the glass particles settle down at the bottom of the channel and roll slowly in

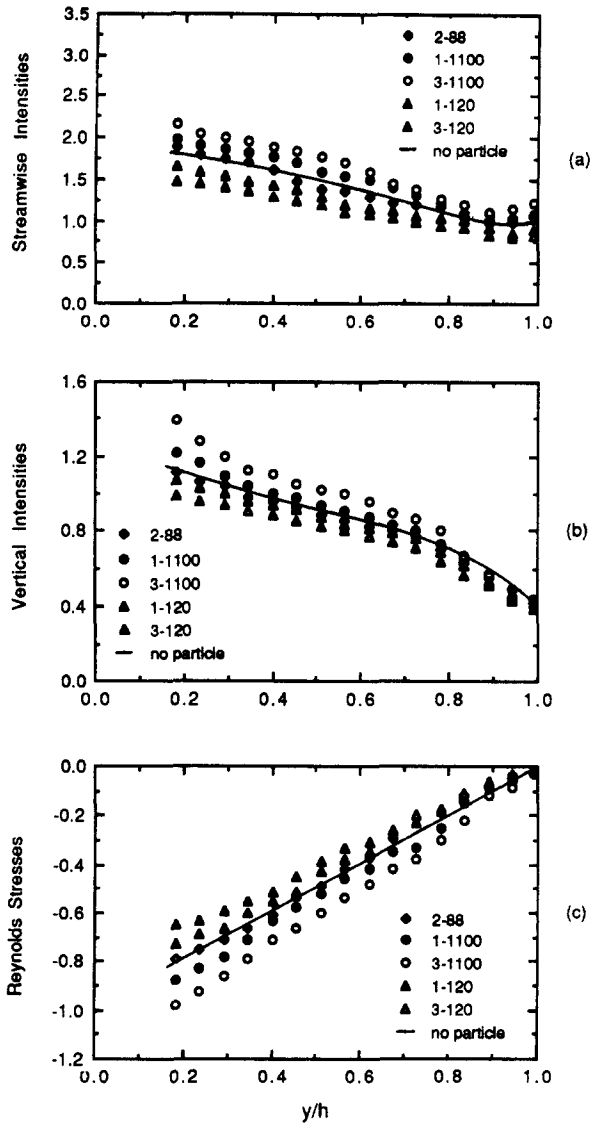

Figure 14. Distributions of dimensionless turbulence intensities. (a) Streamwise intensities; (b) vertical intensities; (c) Reynolds stresses. (Symbols have the same meaning as in Figure 10.)

the direction of the flow. It seems that these particles do not interact with the structures near the wall. They simply roll beneath the active turbulence regions of the wall.

C. *Mechanism of particle transport*

The overall mechanism of particle transport arising from the present experiments and observations of previous investigators (Kline *et al.* 1967; Hinze 1975; Blackwelder & Eckelmann 1979; Rashidi & Banerjee 1990b) is illustrated by figure 15. It appears that the low-speed streaks observed near the wall are formed between pairs of longitudinal counter-rotating vortices. These vortices are elongated in the direction of flow and are separated in the spanwise direction by $\Delta z^+ \approx 50$. The legs of these vortices are inclined at an angle of about 20–25° to the boundary at $y^+ < 20$. As particles are introduced in the flow, they mostly accumulate in the low-speed streaks of the wall structures. These particles are then lifted up (depending on their size and density) by the inclined vortex-loops of the wall regions and are ejected into the bulk flow. The ejected particles, having a density slightly greater than fluid, eventually come back to the wall region. As these particles return to the wall region, some encounter wall ejections already in progress and are lifted up before reaching the wall regions. The bursting process repeats itself causing the transport of the particles in the flow direction.

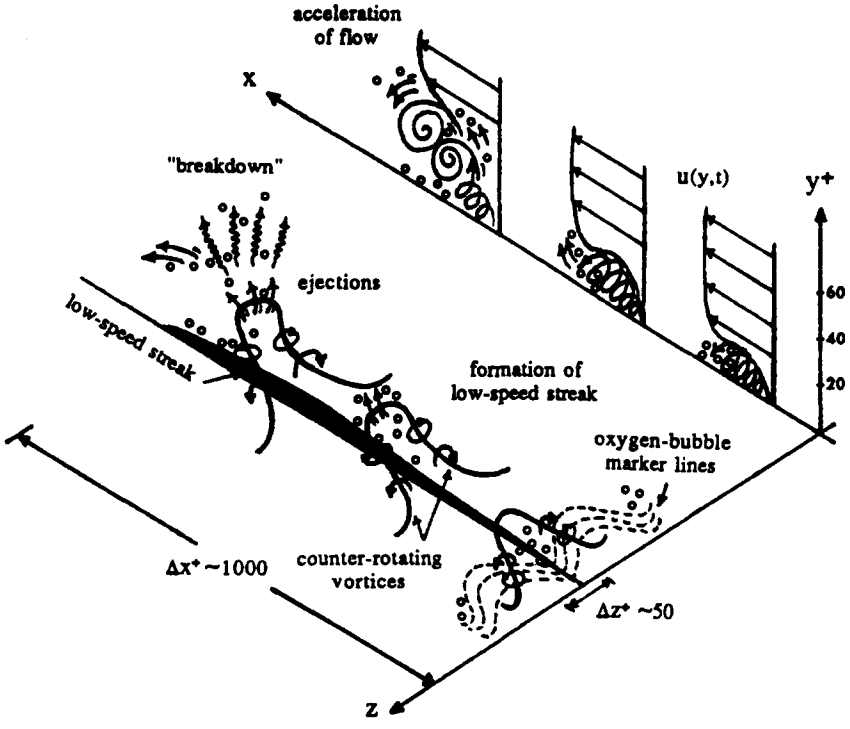

Figure 15. Mechanism of particle transport near the wall.

The present experiments show that the particle–burst interaction is very dependent on the particle density, particle size and flow Re. As the particle diameter decreases below $d^+ \approx 1$, the particles that fell beneath the viscous sublayer do not interact with the bursting process and are rarely lifted up by the wall ejections. Similarly, as the size and density of the particles are increased the angle of liftup and the maximum elevation of the lifted particles decrease. Figure 16 illustrates the measurement of mean particle ejection angle, θ, as a function of particle diameter for Re = 5000. As seen from this figure, the ejection angle increases as the particle size decreases, approaching a value close to the inclination angle of the streamwise vortices (the value of $\theta \approx 20$ to 25° which was observed previously for flows with no particles). Furthermore, when Re is increased, the thickness of the viscous sublayer decreases and, as seen from these experiments, the ejection velocities increase, thus enhancing the particle liftup process.

CONCLUSIONS

Particle–turbulence interaction in turbulent channel flows has been studied via flow visualization. Experiments with changing particle size, particle density, particle loading and flow Re have been conducted. It is found that the larger polystyrene particles ($\sim 1100\ \mu$m dia) cause an increase in

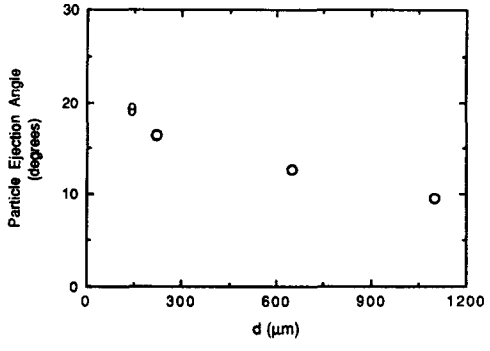

Figure 16. Effect of particle size on the average particle ejection angle, θ, at Re = 5000.

the number of wall ejections, giving rise to an increase in the values of turbulence intensities and Reynolds stresses. While, the smaller polystyrene particles ($\sim 120\ \mu$m dia) cause a decrease in the number of wall ejections, therefore giving rise to a decrease in the intensity and the Reynolds stress measurements. The effects are enhanced as particle loading is increased. It is also shown that the heavier glass particles ($\sim 88\ \mu$m in dia) do not cause any significant change in these results. In addition, measurements of the burst frequency and the mean streak-spacing show no significant change with increased particle loading. The mean streak-spacing appears to be independent of particle loading and exhibits consistent values of $\lambda^+ \approx 100$ at $y^+ = 5$.

Based on these observations, it appears that particle transport is controlled mainly by the ejections originating from the liftup and breakdown of the low-speed streaks in the wall regions. As particles are introduced in the flow, they mostly accumulate in the low-speed streaks of the wall structures. These particles are then lifted up by these structures (depending on their size, density and flow Re) and are ejected into the bulk flow. The ejected particles later return toward the wall, some encountering the wall ejections already in progress get lifted up before reaching the wall regions. So, the bursting process repeats itself and dominates the particle transport, while the particles presence affects the mechanism by which the turbulence energy is transported from the wall region to the bulk flow.

Acknowledgements—This research is supported by the Electric Power Research Institute, Grant No. RP 8006-17, with Dr J. Maulbetsch, Program Manager, and by the National Science Foundation, Grant No. CTS-8822056, with Drs S. Goren and M. Roco, Program Directors.

REFERENCES

BAGNOLD, R. A. 1941 *The Physics of Wind-blown Sand and Desert Dunes.* Methuen, London.

BLACKWELDER, R. F. & ECKELMANN, H. 1979 Streamwise vortices associated with the bursting phenomenon. *J. Fluid Mech.* **94,** 577–594.

CLEAVER, J. W. & YATES, B. 1973 Mechanism of detachment of colloid particles from a flat substrate in turbulent flow. *J. Colloid Interface Sci.* **44,** 464–473.

CLEAVER, J. W. & YATES, B. 1975 A sublayer Model for deposition of the particles from turbulent flow. *Chem. Engng Sci.* **30,** 983–992.

CLEAVER, J. W. & YATES, B. 1976 The effect of re-entrainment on particle deposition. *Chem. Engng Sci.* **31,** 147–151.

DYER, K. R. & SOULSBY, R. L. 1988 Sand transport on the continental shelf. *A. Rev. Fluid Mech.* **210,** 295–324.

GRASS, A. J. 1974 Transport of fine sand on a flat bed: turbulence and suspension mechanics. In *Proc. Euromech., Tech. Univ. of Denmark, Copenhagen,* Vol. 48, p. 33.

HETSRONI, G. 1989 Particles–turbulence interaction. *Int. J. Multiphase Flow* **15,** 735–746.

HINZE, J. O. 1975 *Turbulence,* 2nd edn. McGraw-Hill, New York.

ITAKURA, T. & KISHI, T. 1980 Open channel flow with suspended sediments. *J. hydraul. Div. ASCE* **106**(8), 1325–1343.

KIM, H. T., KLINE, S. J. & REYNOLDS, W. 1971 The production of turbulence near a smooth wall in turbulent boundary layer. *J. Fluid Mech.* **50,** 133–160.

KLINE, S. J., REYNOLDS, W. C., SCHRAUB, F. A. & RUNDSTADLER, P. W. 1967 The structure of turbulent boundary layer. *J. Fluid Mech.* **30,** 741–773.

RASHIDI, M. & BANERJEE, S. 1988 Turbulence structure in free-surface channel flows. *Phys. Fluids* **31,** 2491–2503.

RASHIDI, M. & BANERJEE, S. 1990a The effect of boundary conditions and shear rate on streak formation and breakdown in turbulent channel flow. *Phys. Fluids.* In press.

RASHIDI, M. & BANERJEE, S. 1990b Streak characteristics and behavior near wall and interface in open channel flows. *Trans. ASME Jl Fluids Engng* **112,** 164–170.

ROGERS, C. B. & EATON, J. K. 1989 The interaction between dispersed particles and fluid turbulence in a flat plate turbulent boundary layer in air. Report MD-52, Stanford Univ., Calif.

SNYDER, W. H. & LUMLEY, J. L. 1971 Some measurements of particle velocity autocorrection functions in a turbulent flow. *J. Fluid Mech.* **48,** 41–47.

SOO, S. L., IHRIG, H. K. & EL KOUH, A. F. 1960 Experimental determination of statistical properties of two-phase turbulent motion. *Trans. ASME Jl Fluids Engng* **D82,** 609–624.

SOULSBY, R. L. & WAINWRIGHT, B. L. S. A. 1987 A criterion for the effect of suspended sediment on near-bottom velocity profiles. *J. hydraul. Res.* **25,** 341–356.

SUMER, B. M. & DEIGAARD, R. 1981 Particle motions near the bottom in turbulent flow in an open channel: Part 2. *J. Fluid Mech.* **109,** 311–337.

TAYLOR, P. A. & DYER, K. R. 1977 Theoretical models of flow near the bed and their implications for sediment transport. In *The Sea*, Vol. 6 (Edited by GOLDBERG, E. D., MCCAVE, I. N., O'BRIEN, J. J. & STEELE, J. H.), pp. 579–601. Wiley-Interscience, New York.

WELLS, M. W. & STOCK, D. E. 1983 The effects of crossing trajectories on the dispension of particles in turbulent fluids. *J. Fluid Mech.* **136,** 31–62.

YUNG, B. P. K., MERRY, H. & BOTT, T. R. 1989 The role of turbulent bursts in particle re-entrainment in aqueous systems. *Chem. Engng Sci.* **44,** 873–882.